Cross-Rate Interference and Implications for Core eLoran Service Provision

Jan Šafář[1], Paul Williams[2], Sally Basker[2], František Vejražka[1]

[1] *Czech Technical University, Prague*

[2] *The General Lighthouse Authorities of the UK and Ireland*

Biographies

Mr. Jan Šafář was awarded the degree of Ing. (MEng) by the Czech Technical University in Prague, Czech Republic in 2007. Currently, he is a PhD student in the Department of Radio Engineering at the same university. He became involved in eLoran during a three month study period undertaken at the General Lighthouse Authorities of the United Kingdom and Ireland. His PhD project is focused on Group Repetition Interval Selection and Core eLoran Service Capacity and his current studies are being sponsored by The Corporation of Trinity House. He is a Member of the Royal Institute of Navigation.

Dr. Paul Williams is a Principal Engineer with the Research and Radionavigation Directorate of The General Lighthouse Authorities of the UK and Ireland, based at Trinity House in Harwich, England. As the technical lead of the GLA's eLoran Work Programme, he is involved in planning the GLAs' maritime eLoran trials and works on a wide range of projects from real-time differential-Loran system development to the quality assurance of Loran ASF data. He holds BSc and PhD degrees in Electronic Engineering from the University of Wales, is a Chartered Engineer, an Associate Fellow of the Royal Institute of Navigation and is a board member of the International Loran Association.

Dr. Sally Basker is the Director of Research and Radionavigation for the General Lighthouse Authorities (GLAs) of the United Kingdom and Ireland where she has a key leadership role as the GLAs move from a service mix based primarily on lighthouses and buoys to one based increasingly on radionavigation systems. Prior to her current appointment, Dr Basker worked in the consultancy sector for eight years where she provided strategy, business and technology support to public and private sector clients. Recent achievements have included leading the development of the first GLA Radionavigation Plan, the procurement of a fifteen-year Loran service for the UK and the study for the development of a European Radio Navigation Plan. Dr Basker is a member of the Department for Transport's e-Navigation Strategy Group and a member of the Department for Innovation, Universities and Skills (DIUS) Working Group on Physical Metrology. She is a Fellow of the Royal Institute of Navigation and the President of the International Loran Association. Dr Basker holds Ph.D and B.Eng degrees from the University of Nottingham.

Prof. Ing. František Vejražka, CSc. is a full professor of radio navigation, radio communications and signals and systems theory of Czech Technical University in Prague, Czech Republic since 1996. He participated on the design of the first Czech GPS receiver (1990) for the MESIT Instruments factory. His team prepared experimental receivers for Galileo, GPS and GLONASS based on software radio concept and participated on European 6-th Frame Program project GARDA. Prof. Vejražka has published 11 textbooks, more than 200 conference papers and many technical reports. He is the former president of the Czech Institute of Navigation, Fellow of the Royal Institute of Navigation in London, member of the Institute of Navigation (USA), CGIC/IISC, IEEE, member of Editorial Board of GPS World, Editorial Board of Inside GNSS, etc.

Abstract

According to the *eLoran Definition Document* issued by the International Loran Association, eLoran will be divided into *Core Service Provision* components and *Application Service Provision* components. Core service provision includes eLoran transmitters and their associated monitoring and control infrastructure. Application service provision includes that infrastructure required to support the application requirements of specific user segments.

The accuracy, integrity, availability and continuity performance of eLoran core service provision depends on the number of eLoran transmitters within a coverage area. Recent developments in new technology transmitters have created the potential for cost-effective improvements in eLoran coverage. However, with each additional transmitter installed, more Cross-Rate Interference (CRI) is added to the radio environment within which eLoran stations are expected to operate. This extra interference increases the attendant integrity risk upon signal reception and places a limit on the number of stations that can operate within a specific area. CRI is inherent to the eLoran system and cannot be prevented. Nevertheless, its effect can be mitigated by judicious choice of the *Group Repetition Intervals* (GRIs) within which the stations transmit and by advanced receiver signal processing techniques.

At the NAV08/ILA37 conference we presented a set of Matlab™ tools, which implement a GRI selection technique based on methods sanctioned by the International Association of Marine Aids to Navigation and Lighthouse Authorities (IALA) for the establishment of new Loran-C chains. We also extended the techniques by developing a number of updates that take into account the modernization of Loran-C to the eLoran standard.

In this new paper we continue our investigations and take a closer look at the problem of CRI. We quantify positioning errors introduced by unmitigated CRI. We then demonstrate how CRI can be mitigated in an eLoran receiver by blanking the interfering pulses and we show the impact of the attendant blanking loss on the accuracy performance of eLoran core service provision.

1 Introduction

In recent years, the world of radio navigation has seen a renewed interest in the Loran Positioning, Navigation and Timing (PNT) system, or rather in its upgraded version now

widely called *enhanced Loran* or simply *eLoran* [8]. The main reason that has led to this, perhaps unexpected, resuscitation of an almost forgotten terrestrial low-frequency system is the growing awareness of vulnerabilities [10] [5] [7] of GPS, which is currently the primary source of PNT information in many applications. These vulnerabilities are largely a consequence of the extremely low signal levels at the surface of the Earth and are common to all *Global Navigation Satellite Systems* (GNSS) – present, as well as future.

The eLoran system is perceived by its supporters as a complement and back-up to GNSS. As such, it should deliver a comparable level of performance to that of GNSS – an open challenge for eLoran system designers and receiver manufacturers. Meeting the system performance requirements set out within the *eLoran Definition Document* [8] will likely involve expanding the current Loran transmission network. Today, highly efficient scalable eLoran transmitters are available, affording the possibility of improving performance in high-risk areas. However, with each additional transmitter installed, mutual interference levels are increased within the system. This, so called *Cross-Rate Interference* (CRI) is currently the strongest source of interference to eLoran.

CRI is inherent to the eLoran system and cannot be prevented. Nevertheless, its effect can be mitigated by judicious choice of the *Group Repetition Intervals* (GRIs) within which the stations transmit and by *advanced receiver signal processing techniques*. Some methods of optimal GRI selection for new stations have already been investigated by the authors in [3]. These were based on previous work carried out mainly at Technical University Delft in the early 1990's, when the European Loran-C chains (NELS) were planned. In that time a great deal of attention was paid to the other crucial factor in GRI selection – i.e. the problem of Continuous Wave Interference (CWI). This posed the biggest threat to Loran back then, since Europe was a particularly noisy radio environment. A receiver's susceptibility to CWI depends on the chosen GRI and the current GRI selection method presented in [3] allows ranking of the GRIs according to their sensitivity to this kind of interference. Our current findings suggest that CWI pose no significant threat to eLoran, considering that modern software-defined receivers can implement enough adaptive notch filters to suppress any CWI. The biggest interferer to eLoran is actually eLoran itself in the form of CRI and we therefore turn our attention solely to this problem.

In this current paper, we explore the effect of CRI on the positioning performance of a Loran receiver. The analysis provided herein enables the reader to better understand the nature of CRI, and it forms the basis of an assessment of the effectiveness of modern eLoran receiver CRI mitigation techniques. The ultimate aim of this work, then, is to contribute to the development of an updated GRI selection method that will respect all the major technological benefits delivered by the emerging eLoran system and to help us understand the limitations that CRI places on the core eLoran system provision.

This paper first explains what is meant by CRI and summarises the basics of Loran signal processing needed in the presented analysis. Section 2 deals with the influence of CRI on Loran carrier phase tracking and describes its impact on the accuracy of the position solution. Section 3 looks at CRI blanking – one of the basic methods of CRI mitigation used in modern eLoran receivers. In Section 4, a MATLAB™ Loran signal processing toolbox is briefly described that has been developed in an attempt to verify some of the models derived earlier. Section 5 presents three case studies demonstrating the use of the methods introduced in this paper and finally, in Section 6, some suggestions for future work are given.

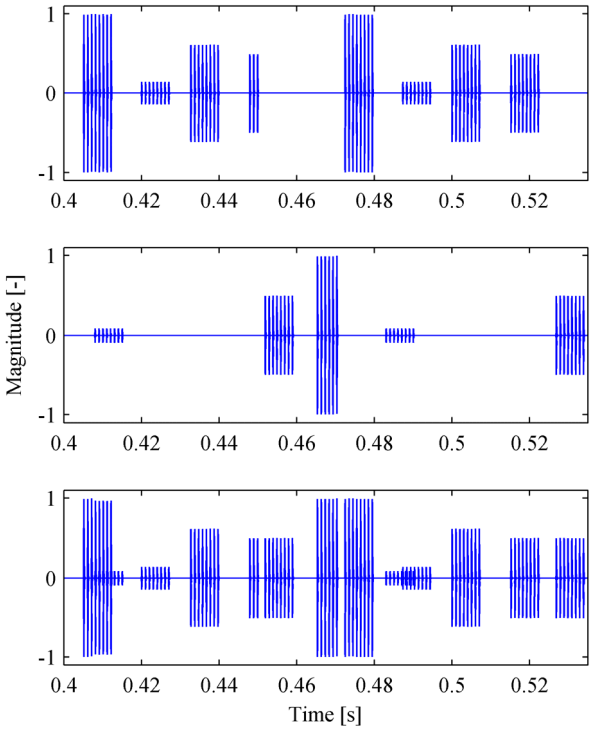

Figure 1: Cross-rate interference between GRIs of 6731 and 7499; upper plot: 6731 Lessay chain (Lessay, Soustons, Anthorn, Sylt); middle plot: 7499 Sylt chain (Værlandet, Sylt, Lessay); bottom plot: composite received signal.

It is assumed in this paper, that the reader is familiar with the basic concepts of Loran systems and the fundamental differences between eLoran and its predecessor – the hyperbolic Loran-C system. Background information on these systems is readily available in the open literature and extensive references can be found for example in [2].

1.1 Key Determinants of CRI

The severity of CRI in a particular location and time depends on many factors, as can be inferred from Equation 1. This equation represents a model of the received Loran signal[1].

$$r(t)=\sum_{k=0}^{K-1}\sum_{m=0}^{M-1}\sum_{c=-\infty}^{\infty}\sum_{j=0}^{7} a_{mk}\, l\left(t-\tau_{mk}-jT_p-c\cdot GRI_k\cdot 10^{-5}\right)\cdot \cos\left(\omega_0 t+\theta_{mk}+PC_{kcj}\right). \quad (1)$$

Here,

K is the number of eLoran stations "in view" and GRI_k are their respective group repetition intervals (in tens of μs);

[1] No noise or external interference is assumed in this model – the primary concern of this analysis is CRI.

$M-1$ is the number of sky waves considered, each with a different amplitude a_m, delay τ_m and phase θ_m ($m=0$ represents the ground wave);

PC_{kcj} are the phase code values (0 or π, according to a standardised pattern), k is the transmitter number, c is the GRI number and j denotes the pulse number within a GRI;

T_p $T_p = 1$ ms;

ω_0 $\omega_0 = 2\pi \cdot 100 \cdot 10^3$ rad/s corresponds to the Loran carrier frequency of 100 kHz; note, that ω_0 is common to all stations;

$l(t)$ $l(t)$ represents the envelope of a single Loran pulse; for $0 < t \le 300$ μs it is given by Equation 2 and $l(t) = 0$ otherwise; t_p is the instant when the pulse reaches its maximum value, $t_p = 65$ μs;

$$l(t) = \left(\frac{t}{t_p}\right)^2 \cdot \exp\left(2 - 2\frac{t}{t_p}\right). \qquad (2)$$

All of the parameters mentioned above play their role in determining the effect of CRI and it can already be seen that thorough analysis of CRI is a very complex task.

Figure 1 shows an example situation in which the signals of 6731 Lessay rate (the upper plot) interfere with those of the 7499 Sylt rate (the middle plot). For reader's convenience, a map showing the positions of the transmitters (Figure 2) is appended, and also Appendix D provides useful information on individual stations considered in this example. Even in the short signal snapshot depicted in Figure 1, several occurrences of CRI can be seen – first, there is a partial *overlap* between the signal groups of 6731 Lessay and 7499 Værlandet stations. This overlap causes a *carrier phase distortion* within the hit pulses, which leads to erroneous pseudorange (and position) measurements in the receiver, as will be explained later. An attentive reader can also notice a slight *envelope distortion* of the pulses from the Lessay station, which occurs as a result of the destructive interference between the signals. And there is another overlap between 7499 Værlandet and 6731 Soustons in Figure 1, but in this case the relative timing of the two groups is such, that the pulses interleave and no errors are likely to occur in the measurements. Another effect of CRI, which can also be seen in this figure is *dual-rate blanking*. Some Loran transmitters are dual-rated, i.e. they broadcast signals on two GRIs (see Appendix D), and such transmitters are periodically faced with the impossible requirement of radiating overlapping pulse groups simultaneously. During the time of overlap, those pulses of one group that overlap any part of the other group' blanking interval are suppressed. The *blanking interval* extends from 900 μsec before the first pulse to 1600 μsec after the last. In Figure 1, blanking of 6731 Sylt and 7499 Lessay signals can clearly be seen.

1.2 Loran Receiver Signal Processing Basics

In order to be able to assess the overall effect of CRI in a particular area it is vital to have certain knowledge about the signal parameters mentioned above. It is, however, no less important to understand the way in which these signals are processed in a Loran receiver to arrive at the position solution. Moreover, modern eLoran receivers utilise advanced signal processing techniques for CRI mitigation and these can change the picture considerably.

Figure 2: Loran transmitters (B/W circles) considered in the example in Section 1.1.

So, how do Loran receivers work anyway? In a sense, they work pretty much in the same way that GNSS receivers do. They identify and lock onto the signals using correlation processing. Then, they make precise measurements of the *Time Of Arrival* (TOA) of the pulses[2] and establish a *pseudorange* from each station "in view" (*all-in-view* concept). The position solution (latitude, longitude, receiver clock offset) can then be obtained using the *Weighted Least Squares* (WLS) method.

The TOA measurements are based on the estimates of the carrier phase of individual Loran ground wave signals[3] and therefore *phase distortions* induced by CRI will be the primary concern of the analysis presented in this paper. However, carrier phase can obviously be measured only "modulo 2π", and as the wavelength of the Loran carrier is "only" 3 km, the receiver needs to resolve this phase ambiguity in order to obtain meaningful TOAs. In Loran jargon, this is referred to as *cycle selection* and during this signal processing stage, the receiver makes coarse TOA estimates[4] based just on the shape of the Loran pulse envelope (Equation 2). In order to resolve the phase ambiguity successfully, the error in the coarse TOA estimate needs to be smaller than 5 μs (i.e. a half-cycle of the Loran carrier). In this way, all Loran timing measurements are related to a standard reference point in the Loran pulse – the *Standard Zero Crossing* (SZC), which is the 6th zero crossing after the start of the pulse. Since CRI can cause pulse envelope distortions, it can also negatively influence the cycle selection function of the receiver, which can in turn result in pseudorange errors in multiples of 3 km. Investigation of the probability of wrong cycle selection due to CRI, however, is beyond the scope of this paper and is left for later work.

[2] More appropriately – groups of pulses – as integration of the signal is necessary to achieve sufficient SNR values.

[3] $\hat{\theta}_{0k}$

[4] $\hat{\tau}_{0k}$

2 Unmitigated CRI and Loran Carrier Phase Tracking

This section follows the work of Zeltser and El-Arini [25], and supplements it by introducing an illustrative vector (or phasor) representation of the problem. In [25], the impact of CRI on the track mode is estimated using a time-domain analysis, which was validated by comparing with the performance of various commercial Loran-C receivers.

2.1 Assumptions

In order to make the herein presented analysis feasible, the following assumptions and simplifications have been made:

- Only ground wave Loran signals are modelled. This assumption allows treating the signals as deterministic.
- Only carrier phase measurement distortion is analysed. The probability of wrong cycle selection due to CRI will be investigated in later |work.
- Phase measurements are made at the SZC.
- The influence of the ninth Master Loran pulse, as well as any data modulation of the signals is ignored.
- Modern receiver CRI mitigation techniques are not taken into account. This section only concentrates on the basic principles behind Loran position measurements, and in that sense it provides the *worst-case estimate* of the effects that CRI can have on the position solution.
- Atmospheric noise and other sources of interference are not taken into account in this section. This analysis shows purely the effect of CRI.
- The errors in the TOA measurements are assumed to be uncorrelated and inaccuracies in system timing (e.g. due to two-way Loran propagation measurement method employed at the Control Center Brest or due to transmitter jitter) are not modelled here.

2.2 Tracking Error versus Time

From what has already been said, it is clear that carrier phase measurements will be at the heart of this analysis. The standard way of estimating carrier phase is to decompose the received signal into its *in-phase and quadrature components* (complex envelope). The phase of the signal is then related to the quotient of the in-phase and quadrature component values. However, Loran is a pulsed system and therefore the phase can be measured only in certain time instants, when the wanted signal is actually present[5]. For a number of practical reasons, the phase of the Loran carrier is usually measured near the 6th zero crossing from the start of the pulse (SZC). The situation can be depicted as in Figure 3. The horizontal and vertical axes represent the in-phase and quadrature components, respectively. In this diagram, each single Loran pulse can now be assigned a vector, which shows the magnitude of the pulse envelope at a specified sampling time and the carrier phase of that particular pulse relative to some reference signal in the receiver.

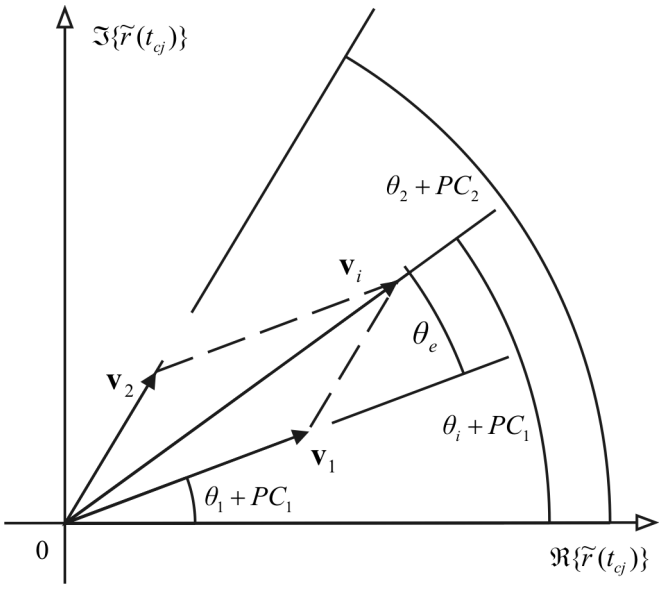

Figure 3: Example phasor diagram showing wanted signal and CRI. Horizontal and vertical axes show real and imaginary part of the complex envelope of the received signal (in-phase/quadrature components), respectively, sampled at a time instant t_{cj}.

Let us consider a specific time instant[6]:

$$t_{cj} = c \cdot GRI_1 \cdot 10^{-5} + j \cdot T_p + t_{SZC} \text{ s}, \quad (3)$$

that corresponds to the SZC of one of the pulses on GRI_1 and explore what happens if another – interfering – Loran pulse is present in the received signal at the same time. In Figure 3, $\mathbf{v}_1$ can represent the wanted signal and $\mathbf{v}_2$ the interfering one. The image of the resulting signal $\mathbf{v}_i$, as seen by the receiver, is then merely a vector addition of the two.

What is of interest in the context of receiver tracking performance is the angle denoted as θ_e. This angle is the phase error caused by the interfering signal per one desired pulse, and according to [25] it can be calculated as follows[7]:

$$\theta_e = \arctan\left\{\frac{m\sin(\theta_2 - \theta_1 + PC_2 - PC_1)}{1 + m\cos(\theta_2 - \theta_1 + PC_2 - PC_1)}\right\}, \quad (4)$$

$$m = \frac{a_2 l(t_{SZC} - d_{cj})}{a_1 l(t_{SZC})}. \quad (5)$$

Here, a_1 and a_2 are the amplitudes of the desired and the interfering signals at the peak of the envelope, respectively; $l(t)$ is the envelope of the Loran pulse as given by Equation 2 and d_{cj} denotes the time delay between the desired pulse and the nearest interfering pulse for the time instant t_{cj}. Since the signals are assumed to be deterministic, the values of this delay at a particular location can be deduced directly from the definition of these signals (Equation 1). By iterating over a certain time interval, an ensemble of phase measurement errors can be collected and used to investigate the effects of CRI.

[5] It is a purpose of the acquisition and cycle selection stages to identify these instants correctly and the impact of CRI on this receiver functionality will not be investigated here.

[6] $t_{SZC} = 30 \cdot 10^{-6}$ s

[7] The same formulae were obtained by solving the geometrical problem in Figure 3.

In a real receiver, however, the pulses are corrupted by heavy atmospheric noise and have to be *averaged* for a certain amount of time to achieve sufficient *Signal-to-Noise Ratio* (SNR). The receiver also performs a *correlation* operation with a phase code sequence defined by the signal specification [22]. The result of these operations is that the pulses from one specific station are coherently added to make one averaged pulse. The average phase error due to CRI after correlating with the corresponding phase code sequence can be calculated as follows:

$$\theta_g = \arctan\left\{\frac{\sum_{n=1}^{16}\rho_n \sin(\theta_{e,n})}{\sum_{n=1}^{16}\rho_n \cos(\theta_{e,n})}\right\}, \qquad (6)$$

$\theta_{e,n}$ designates the phase error at the sampling point corresponding to the n-th pulse of the desired signal in the considered ensemble of measurements; ρ_n is given by Equation 7, again, evaluated at the time instant corresponding to the sampling point of the n-th pulse.

$$\rho = \sqrt{1 + m^2 + 2m\cos(\theta_2 - \theta_1 + PC_2 - PC_1)} \qquad (7)$$

The value of ρ_n is related to the magnitude[8] of the resulting vector, obtained as a vector addition of the n-th desired pulse vector and an interfering pulse vector (if there is any interfering pulse present in the n-th measurement). The right hand side of Equation 6 is in fact nothing other than the phase of a vector formed as a vector addition of the individual error vectors corresponding to the measurement errors in the considered ensemble.

In [25] the average phase error θ_g is then filtered by an output low pass filter, which smoothes the measurement errors but permits sufficiently high bandwidth for the receiver to follow the navigation signal accurately. The tracking error (in µs) is calculated from the filtered phase error, θ_{g0}, as:

$$\Delta t_{g0} = \theta_{g0} \cdot \frac{10}{2\pi}. \qquad (8)$$

The analysis described above allows plotting of the tracking error versus time (see Figure 4) and can be used to estimate the statistics of the errors due to CRI. The values of these statistics (mean, variance) obtained by this method compare very well with experimental data measured on commercial Loran-C receivers, as was shown in [25].

2.3 Estimating the Error Statistics

As long as only ground wave signals are taken into account CRI can largely be considered a deterministic phenomenon. This is because as the transmitted signal waveforms are known, both signal amplitudes and propagation delays are relatively stable in time and they can be modelled with reasonable accuracy. Also, the individual Loran signals are periodic in $2 \cdot GRI$ and so the overlapping patterns between them are periodic too. This provides us at least some comfort in this jumble of variables – with no loss of accuracy, the analysis of CRI can be restricted to a well-defined time interval T_o, referred to as the *overlap time*, after which the CRI-induced errors repeat themselves. The overlap time for two GRIs can be calculated as:

$$T_o = \mathrm{lcm}(2 \cdot GRI_1, 2 \cdot GRI_2) \cdot 10^{-5} \text{ s}, \qquad (9)$$

where $\mathrm{lcm}(.)$ denotes the least common multiple operation.

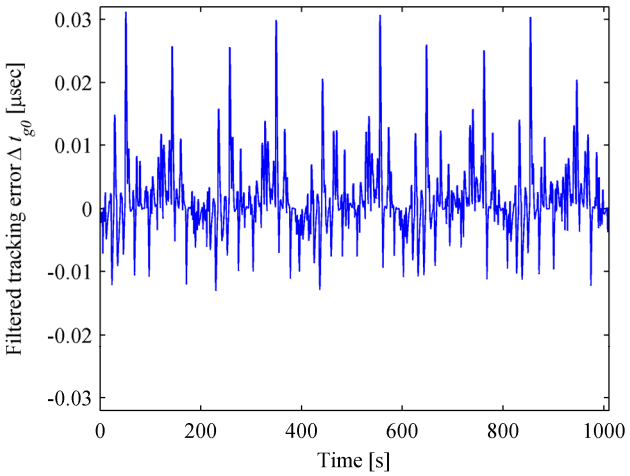

Figure 4: Filtered tracking error due to CRI for the 6731 Lessay station interfering with the signals of the 7499 Sylt chain; the time span equals to the overlap interval of the two GRIs.

Hence, if tracking error statistics in the time domain are to be found, the CRI analysis presented above can be employed to calculate tracking error values over the overlap time between the investigated GRIs and the statistics can be estimated from this limited dataset without any loss of accuracy.

In further analysis, the mean value of the tracking error and its variance will be of interest. More appropriately, the mean and variance of the error in the pseudorange measurements, which can be obtained from the tracking error by multiplying with the signal propagation speed.

2.4 Impact on the Position Solution

This section explains how the tracking error (or the error in pseudoranges) translates into the position domain and demonstrates how the error statistics estimated earlier can be used to evaluate the impact of CRI on the accuracy of the position solution.

Estimating User's Position

The standard Loran position algorithm applies the WLS method to an over-determined set of range measurements. Starting with an initial position estimate, an iterative computation finds a position, which minimises the square of the differences between the measured ranges (pseudoranges) to the stations and the ranges computed from the current estimated position. The corrections in user's position $\Delta x, \Delta y$ and clock offset Δb_u are calculated in each iteration of the algorithm as follows:

$$\Delta \mathbf{u} = \left(\mathbf{A}^{\mathrm{T}}\mathbf{W}\mathbf{A}\right)^{-1}\mathbf{A}^{\mathrm{T}}\mathbf{W}\Delta\boldsymbol{\rho}, \qquad (10)$$

[8] $\left|\mathbf{v}_{i,n}\right| = a_1 I(t_{cj})\rho_n$

$$\Delta\mathbf{u} = \begin{pmatrix} \Delta x \\ \Delta y \\ \Delta b_u \end{pmatrix}. \quad (11)$$

In Equation 10, $\Delta\boldsymbol{\rho}$ is a column vector of differences between observed pseudoranges and pseudoranges computed from the current estimated position using a certain signal propagation model. Matrix $\mathbf{W}$ is a *weight matrix*. Each station's contribution is weighted according to a measure of signal quality, which allows the most accurate measurements to have the greatest influence on the solution. Finally, matrix $\mathbf{A}$ is a *direction cosine matrix* and it describes the geometry of Loran stations relative to the user's position (see Appendix A).

Impact on the Position Accuracy

The aim of this analysis is to evaluate the impact of CRI on Loran position accuracy. But what is actually meant by the *accuracy* of a positioning system? There are many different position accuracy measures, e.g. root-mean-square (RMS), twice the distance root-mean-square (2DRMS), circular error probable (CEP), 95 percent radius (R95), and so on. The aptly named article [23], *"GPS Accuracy: Lies, Damn Lies, and Statistics",* summarises the problem nicely. As will be shown shortly, the RMS accuracy is a convenient choice for the presented analysis, as it can be calculated easily from the tracking/pseudorange error statistics.

$$\delta_{RMS} = \sqrt{\mathrm{E}\left[\mathrm{dist}^2(\hat{\mathbf{p}}, \mathbf{p})\right]}. \quad (12)$$

In the above definition of RMS accuracy, $\mathrm{dist}(\hat{\mathbf{p}}, \mathbf{p})$ denotes the distance between the estimated position and the true position of the receiver. Loran position calculations are normally made using geodetic (latitude, longitude) coordinates. When investigating accuracy, however, only small position deviations relative to a reference point are of interest. It is then possible to approximate Earth's surface by a local tangent plane and use Cartesian instead of the, computationally rather cumbersome, geodetic coordinates. Equation 12 can then be rewritten as follows:

$$\delta_{RMS} = \sqrt{\mathrm{E}\left[\left(\underbrace{\hat{x} - x}_{\Delta x}\right)^2 + \left(\underbrace{\hat{y} - y}_{\Delta y}\right)^2\right]} = \sqrt{\mathrm{E}\left[\Delta x^2\right] + \mathrm{E}\left[\Delta y^2\right]}. \quad (13)$$

Further, using the well-known equality:

$$\mathrm{var}(\Delta x) = \mathrm{E}\left[\Delta x^2\right] - \mathrm{E}^2\left[\Delta x\right], \quad (14)$$

the RMS accuracy can be expressed in terms of the mean and variance of the corrections in user's position:

$$\delta_{RMS} = \sqrt{\mathrm{var}(\Delta x) + \mathrm{E}^2\left[\Delta x\right] + \mathrm{var}(\Delta y) + \mathrm{E}^2\left[\Delta y\right]}. \quad (15)$$

The question now is how to calculate these, based on the estimated statistics of the pseudorange errors caused by CRI. The answer can be found by examining Equation 10. It can be shown (see Appendix B) that the variance of the corrections in the position solution $\Delta\mathbf{u}$ is minimised, when the weight matrix is equal to an inverse of the *measurement covariance matrix:*

$$\mathbf{W} = \mathbf{R}^{-1}, \quad (16)$$

$$\mathbf{R} = \begin{pmatrix} \sigma_1^2 & 0 & 0 \\ 0 & \ddots & 0 \\ 0 & 0 & \sigma_K^2 \end{pmatrix}. \quad (17)$$

This matrix contains the variances σ_i^2 on each TOA measurement. A method for estimating the variances on TOAs due to CRI has been presented in Section 3. If Equation 16 holds, then:

$$\mathrm{var}(\Delta\mathbf{u}) = \left(\mathbf{A}^{\mathrm{T}}\mathbf{R}^{-1}\mathbf{A}\right)^{-1}. \quad (18)$$

The mean value can be calculated as:

$$\mathrm{E}\left[\Delta\mathbf{u}\right] = \left(\mathbf{A}^{\mathrm{T}}\mathbf{R}^{-1}\mathbf{A}\right)^{-1}\mathbf{A}^{\mathrm{T}}\mathbf{R}^{-1}\,\mathrm{E}\left[\Delta\boldsymbol{\rho}\right]. \quad (19)$$

From the results of the above calculations, the quantities needed to compute the RMS accuracy according to Equation 15 can be extracted directly. Accuracy is often expressed as a 2DRMS value, which is calculated simply as $\delta_{2DRMS} = 2 \cdot \delta_{RMS}$.

All the necessary mathematical tools for the CRI analysis are now available. Based on the timing relations between the signals of individual Loran stations and their amplitudes at a specified location, it is possible to evaluate tracking error waveforms, estimate the pseudorange error statistics and finally arrive at the RMS position error due to unmitigated CRI for that location. Section 5 presents two example studies on the effect of unmitigated CRI.

3 CRI Blanking and Blanking Loss Evaluation

As can be seen from the analysis contained in Section 5 of this paper, uncompensated CRI constitutes a potent source of interference to Loran. In order to meet the stringent eLoran accuracy performance standards determined by the needs of the maritime sector, it is necessary that eLoran receivers employ some CRI mitigation algorithms. Several strategies concerning how the receiver can reduce the effect of CRI have been described in the literature [17]. In this paper we deal with one of these techniques, commonly referred to as *"CRI blanking"*. With this technique, the eLoran receiver *detects* the pulses likely corrupted by CRI *and discards* them. Two CRI detection mechanisms are known:

- Comparing the received pulses with a reference pulse shape obtained as a moving average of pulses from recent GRIs.
- If the receiver tracks the signals of the stations causing CRI, it can calculate the time instants when the pulses overlap beforehand, based on the known timing relations among the signals.

This approach to CRI mitigation theoretically achieves the best reduction of CRI-induced noise, as all the pulses hit by CRI are eliminated and the receiver makes use of the healthy, undistorted, pulses only. However, in practice, the percentage of discarded pulses may be rather high, which means that SNR of the desired signals may drop significantly. In the rest of this section, we present methods of evaluating this blanking loss. In Section 5 we then use these methods to show the impact of CRI blanking on the accuracy performance of eLoran core service provision.

3.1 Assumptions

The first four assumptions made in Section 2 remain valid. We will however include atmospheric noise and transmitter related noise into our considerations in this section.

3.2 Evaluating the Blanking Loss

Brute Force Approach

CRI resulting from ground wave signals is largely deterministic and can be well predicted. We have already seen that the overlapping patterns between two interfering signals with rates GRI_1, GRI_2 are periodic in T_o - the overlap time (Equation 9). Calculation of the attendant blanking loss, then, can be accomplished in a straightforward manner by generating the two pulse trains and counting the number of overlapping pulses on an interval equal to T_o. Similar to [11], we model the desired pulses as windows of width $w_d = 60$ μsec and the interfering pulses as $w_i = 300$ μsec. The lower and upper edges of individual windows for the wanted signal are defined by the following equations:

$$t_{cj,lo} = c \cdot GRI_1 \cdot 10^{-5} + j \cdot T_p + d_0, \tag{20}$$

$$t_{cj,up} = t_{cj,lo} + w_d, \tag{21}$$

where d_0 is the initial time offset between the two interfering signals at the user's position, determined by the emission and propagation delays of the signals. For each pulse within the overlap interval we evaluate $t_{cj,lo}$ and $t_{cj,up}$ modulo GRI_2 and declare a hit whenever at least one of these values falls within one of the windows that correspond to the pulses of the interfering signal. These are intervals I_k, defined as follows:

$$I_k = \langle k \cdot T_p, k \cdot T_p + w_i \rangle, \quad k = 0 \ldots 7. \tag{22}$$

The blanking loss, L_b, is a ratio of the number of hit pulses to the total number of pulses of the wanted GRI per overlap interval.

As can be inferred from Equation 20, the number of hit pulses per overlap interval changes with the value of the initial offset d_0, i.e. with the user's position. This is illustrated in Figure 5, which shows the values of blanking loss for two specific GRIs and different d_0 values. It is also apparent that the pattern in Figure 5 is periodic and it can be shown that the period is equal to the greatest common divisor of the two GRIs. The advantage of this method of blanking loss evaluation is that it gives us exact results for any specified value of d_0. However, the calculations usually involve testing of tens of thousands of pulses and can be rather time consuming. Therefore, other methods have been sought.

Statistical Approach

Finding an analytical solution to the pulse coincidence problem described above has proved to be a surprisingly challenging task, which had been tackled by many researchers before. In particular, we have found the work of Stein and Johansen [20] and Self and Smith [19] very useful. In [20] the

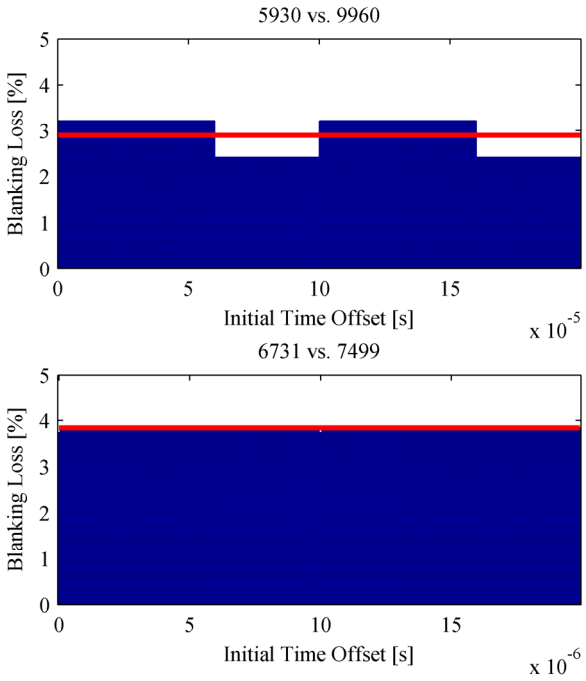

Figure 5: Blanking loss as a function of the initial time offset for GRI 5930 interfering with GRI 9960 (upper plot) and GRI 6731 interfering with GRI 7499 (bottom plot); the red line shows the mean value over all possible time offsets.

authors presented an elegant method for describing statistically the time coincidences among a set of random pulse trains. The important result of that paper is the derivation of a statistical distribution for the durations of the coincidences, when a similar distribution is known for the pulse lengths in the individual pulse trains. This method was later used in [19] to derive an expression for T_c, the mean period of simultaneous overlaps of K pulse trains, each of which is defined by the mean pulse duration, w_k, and mean pulse period T_k:

$$T_c = \frac{\prod_{k=1}^{K}\left(\frac{T_k}{w_k}\right)}{\sum_{k=1}^{K}\left(\frac{1}{w_k}\right)}. \tag{23}$$

For two signals the formula reduces to:

$$T_c = \frac{T_1 \cdot T_2}{w_1 + w_2}. \tag{24}$$

Hence, on average, we have $1/T_C$ collisions per second and if we multiply this by the average pulse period of the desired signal, T_1, we get the percentage of blanked pulses from pulse train 1, i.e. the blanking loss:

$$L_b = \frac{w_1 + w_2}{T_2}. \tag{25}$$

For two eLoran signals, using the notation established above, this can be rewritten as:

$$L_b = \frac{n_2\left(w_d + w_i\right)}{GRI_2 \cdot 10^{-5}}, \tag{26}$$

where n_2 is the number of pulses per GRI of the interfering signal. We can see that the problem is in fact equivalent to considering two pulse trains, one with a pulse duration $w_d + w_i$ and the other with infinitesimally small duration and period $T_2 = GRI_2 \cdot 10^{-5} / n_2$. Pulses from train 2 occur every T_2, hence the probability of overlap for a given pulse from train 1 is governed by Equation 26. The rigorous derivation contained in [20] and [19] proves that such a simplification is justified and it shows that our equations are equally valid for random and regular pulse trains. For random pulse trains, T_k and w_k are mean values; for regular trains, such as eLoran signals, they are specific, well-defined, values.

Equation 26 allows a considerable simplification of the blanking loss calculations compared to the previous "brute force" method. It was however assumed during the derivation of the above equations that the phases of our signals are random. Therefore we are unable to calculate the exact blanking loss values for specific initial time offsets between the signals using this statistical method. Instead, the results obtained from Equation 26 represent the *mean value of blanking loss* over all possible time offsets, i.e. over all d_0 in Equation 20. This is also illustrated by the red line in Figure 5. Note, however, that for those GRIs that are mutually prime[9] there is practically no variation in the blanking loss with changing time alignment of the two signals and the true value of blanking loss at a specific location can be very well approximated by the average value calculated according to Equation 26.

Number-Theoretic Approach

Not entirely satisfied by our partial success in the field of statistics we decided to explore other branches of mathematics, which could provide tools for computationally efficient and exact solution to the coincidence problem. We have found such tools in the part of mathematics called "number theory", specifically, use will be made of the theory of *linear congruences*.

The concept of linear congruences was successfully applied to the pulse coincidence problem by Miller and Schwarz in [14]. In that paper, the authors explain the fundamental properties of congruences and use them to determine the coincidence time fraction for two pulse trains with both a fixed initial phase and a randomly varying phase. Their method was further refined by Friedman [6] and can now be restated as follows, in a way that does not require any special knowledge of number theory:

Consider two regular pulse trains PT1, PT2, according to Figure 6. In accordance with [14] we shall assume that all values in our analysis are integral multiples of some number p:

$$\begin{aligned} p_1 &= \mu p \quad T_1 = mp \\ p_2 &= \nu p \quad T_2 = np \\ s &= rp. \end{aligned}$$

Let $g = \gcd(m,n)$ and $M = lcm(m,n)$. We form all possible differences $x_2 - x_1$, where

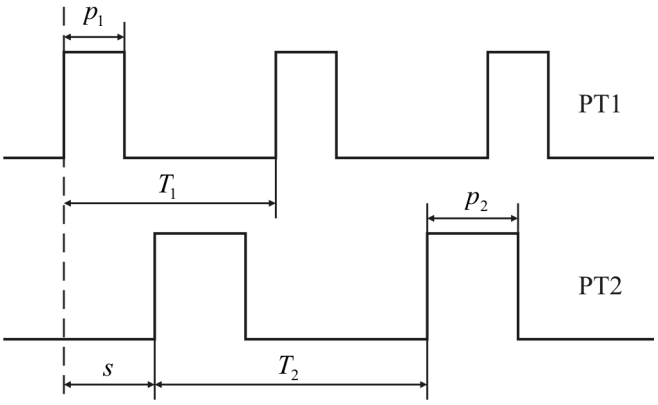

Figure 6: Two pulse trains.

$$\begin{aligned} x_1 &= 1, 2, \ldots, \mu \\ x_2 &= r+1, r+2, \ldots, r+\nu. \end{aligned} \tag{27}$$

Let N be the number of these differences which are divisible by g. The time fraction of coincidence of the two pulse trains is then [6]:

$$f = \frac{N}{M}. \tag{28}$$

Friedman [6] derived an effective method of calculating N in Equation 28, following the pattern of Table 1. This table shows all differences $x_2 - x_1$, which satisfy the above condition, in the special case that $r = 0$ (i.e. zero initial time offset between PT1 and PT2). The quantities a_1, a_2, r_1, r_2 in this table are defined as follows:

$$\begin{aligned} \mu &= a_1\, g + r_1 \quad 0 \le r_1 < g \\ \nu &= a_2\, g + r_2 \quad 0 \le r_2 < g, \end{aligned} \tag{29}$$

a_1, a_2 are integers.

More importantly for our purposes, Friedman's technique also allows us to calculate the exact number of overlapped pulses per overlap time of PT1 and PT2. This can be achieved by considering the following:

The left edge of each overlap is determined by the left edge of some pulse in one, or both, of our pulse trains. Since Table 1 is essentially a description of all units of coincidence of the two pulse trains PT1, PT2 [6], each occurrence of $x_1 = 1$ in that table can be interpreted as an overlap in which the left edge of the PT1 pulse participates. Analogically for $x_2 = 1$ and PT2. The total number of overlaps per overlap time, k_{12}, is then:

$$k_{12} = n_1 + n_2 - 1, \tag{30}$$

where n_i is the number of occurrences of $x_i = 1$ in Table 1. We subtract 1 from $n_1 + n_2$, as we have counted the overlap corresponding to $x_1 = 1, x_2 = 1$ twice. As shown in [6], the values of n_1 and n_2 for $r = 0$ can be deduced directly from Table 1.

[9] all current European GRIs are mutually prime

x_2	x_1	Total per row
1	$1, 1+g, 1+2g, \ldots, 1+a_1 g$	a_1+1
2	$2, 2+g, 2+2g, \ldots, 2+a_1 g$	a_1+1
⋮	⋮	⋮
r_1	$r_1, r_1+g, r_1+2g, \ldots, r_1+a_1 g$	a_1+1
r_1+1	$r_1+1, r_1+1+g, \ldots, r_1+1+(a_1-1)g$	a_1
⋮		⋮
g	$g, 2g, 3g, \ldots, a_1 g$	a_1
$g+1$	$1, 1+g, 1+2g, \ldots, 1+a_1 g$	a_1+1
⋮	⋮	⋮
	etc.	

Table 1: Friedman's pattern for calculation of the coincidence fraction.

We now extend the method to allow for an arbitrary value of r, i.e. arbitrary initial time offset between the pulse trains. We need to find a pattern similar to Table 1, which will enable us to evaluate n_1 and n_2 effectively; n_1 is again the number of occurrences of $x_1 = 1$ in our pattern, but n_2 is now the number of occurrences of $x_2 = r+1$ (recall Equation 27).

For reasons that will be apparent later, we define:

$$\begin{aligned} \mu &= a_1\, g + r_1 && 0 \le r_1 < g \\ r+1 &= a_1' g + r_1' && 0 \le r_1' < g \\ r+\nu &= a_2'\, g + r_2' && 0 \le r_2' < g \\ r &= a_2''\, g + r_2'' && 0 \le r_2'' < g \end{aligned} \tag{31}$$

a_i, a_i', a_i'' are integers. Let us now calculate n_1, i.e. the number of differences $x_2 - x_1$ which are divisible by g and in which $x_1 = 1$ participates. We will do this in two steps. We know that x_2 is in the range $r+1$ to $r+\nu$ (Equation 27). Let us however assume that x_2 can take on all integer values between 1 and $r+\nu$ first. In that case the values of x_2 that satisfy the above condition on the difference $x_2 - x_1$ can be written as:

$$x_2 : 1, 1+g, 1+2g, \ldots, \begin{cases} 1+a_2' g & \text{if } r_2' > 0 \\ 1+(a_2'-1)g & \text{if } r_2' = 0. \end{cases}$$

We can see that there are n_1' values of x_2 that satisfy our condition, where:

$$n_1' = \begin{cases} a_2'+1 & \text{if } r_2' > 0 \\ a_2' & \text{if } r_2' = 0. \end{cases} \tag{32}$$

Now, let us assume that x_2 takes on all integer values between 1 and r. In a similar fashion as above, we can find out that there are n_1'' values that satisfy the condition on $x_2 - x_1$, where:

$$n_1'' = \begin{cases} a_2''+1 & \text{if } r_2'' > 0 \\ a_2'' & \text{if } r_2'' = 0. \end{cases} \tag{33}$$

Hence, for x_2 in the range $r+1$ to $r+\nu$, the total number of differences that satisfy our condition, n_1, is given by:

$$n_1 = n_1' - n_1''. \tag{34}$$

Let us now evaluate n_2, the number of occurrences of $x_2 = r+1$ in our integer model of overlaps. We will enumerate all permissible values of x_1, which result in differences $x_2 - x_1$ divisible by g. If $r_1' > 0$, these values are

$$x_1 : r_1',\ r_1'+g,\ r_1'+2g, \ldots, \begin{cases} r_1'+a_1 g & \text{if } r_1 \ge r_1' \\ r_1'+(a_1-1)g & \text{if } r_1 < r_1'. \end{cases}$$

If $r_1' = 0$, then

$$x_1 : g,\ 2g, 3g \ \ldots, a_1 g.$$

From the above we can see that:

$$n_2 = \begin{cases} a_1+1 & \text{if } r_1 \ge r_1' \\ a_1 & \text{if } r_1 < r_1' \text{ or } r_1' = 0. \end{cases} \tag{35}$$

Finally, we are ready to calculate k_{12}, the total number of overlaps per overlap time of PT1 and PT2:

$$k_{12} = \begin{cases} n_1+n_2 & \text{if } g \text{ does not divide } r \\ n_1+n_2-1 & \text{if } g \text{ divides } r. \end{cases} \tag{36}$$

(If r is divisible by g then the combination $x_1 = 1$, $x_2 = r+1$, has been counted twice and we must subtract 1 from n_1+n_2).

So far in this subsection we have been dealing with simple pulse trains (SPTs) having exactly one pulse per period. The presented method can, however, be applied to eLoran signals as well. The easiest way to do this seems to be to model each eLoran pulse train as an 8-tuple of time-shifted SPTs. The total number of overlaps per overlap time of two eLoran signals can then be calculated as follows:

$$k_{12,eLoran} = \sum_{i=1}^{8} \sum_{j=1}^{8} k_{ij}\,, \tag{37}$$

where k_{ij} is the number of overlaps between the i-th SPT of the first eLoran signal and j-th SPT of the second eLoran signal, calculated according to Equation 36.

Equations 31 to 37 thus provide a method for rapid calculation of the total number of overlapped pulses over the common period of two pulse trains, yet they give us exact results for any given value of the initial time offset between the signals. In this way, we can avoid iteration over individual pulses, which is needed with the "brute force" approach and which is relatively expensive from a computational perspective.

Other Considerations

In the analysis of real-world eLoran systems we will need to evaluate the *blanking loss due to multiple interferers*. To avoid mathematical complications, we model this as an additive effect. Such an approach is justified in the case of multiple interferers from a common chain, as these cannot overlap. For interfering signals from multiple chains this model provides an upper-bound on the total blanking loss.

As was explained in Section 1.1, there is also a loss of signal due to *dual-rate blanking*. In Europe, dual-rated transmitters use priority blanking, where the same rate is

always blanked at every overlap (the priority rate is not affected). Transmitter blanking can be modelled using the same approaches as those described above; we only need to adjust the pulse-width of the interfering (priority) signal to match the length of the blanking interval (see Section 1) and change the number of "pulses" per period of this signal to 1.

3.3 Impact of Blanking on the Position Solution

In Section 2.4 we explained how the accuracy of the position solution can be evaluated if the error statistics of pseudorange measurements are known. The two biggest sources of measurement error in Loran systems are unmitigated CRI and atmospheric noise. The errors introduced by uncompensated CRI were explored earlier in this paper. We can mitigate the devastating effects of CRI by blanking the overlapping pulses; the more pulses we blank, however, the higher is the influence of atmospheric noise on our measurements, as the signal power available for tracking can decrease significantly. How large are the errors caused by atmospheric noise and how much are these increased as a result of blanking then?

The traditional approach to atmospheric noise modelling for Loran makes use of the ITU model [9]. This model can be used to calculate the *RMS atmospheric noise field strength at any percentile* required at a given geographical point and frequency and for certain noise bandwidth of the receiver. At higher levels, the character of the atmospheric noise is more and more impulsive. It can be shown [4], that non-linear signal processing[10] can mitigate the effect of highly impulsive noise. Loran researchers therefore usually introduce some *credit for non-linear processing*. According to [13], a 12 dB credit represents a conservative estimate for noise levels above 80 percentile and this value will also be used in this paper.

Using the ITU noise model and some ground wave propagation model we can calculate Signal-to-Noise Ratio (SNR) estimates for all eLoran stations assumed in our analysis. In this paper we use software tools developed by Williams to do this [24]. Ground wave propagation predictions are based on Millington's method. These calculations give us SNR values for a single pulse. *Averaging* of the signals, which is necessary to achieve sufficient SNR, is taken into account as shown in Appendix C. When calculating the processing gain due to averaging, however, we have to account for the effect of blanking. We describe this effect by means of an *SNR debit due to blanking*, D_b [dB], which can be approximately calculated as follows (see Appendix C):

$$D_b \approx 10\log_{10}\frac{1}{1-L_b}, \qquad (38)$$

where L_b [-] is the blanking loss experienced by the receiver at a particular location, calculated using one of the methods described in Section 5.

The SNR values calculated for individual stations can now be converted into pseudorange variations. A number of models have been derived for this purpose; we will use the model presented by Lo in [12]:

[10] such as clipping, which is always present due to a finite range of AD converters in the receiver

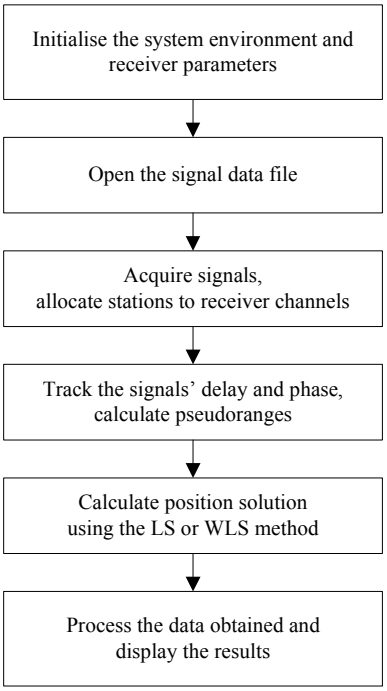

Figure 7: Basic diagram of the Loran signal processing tool.

$$\sigma_i^2 = c_1 + \frac{337.5^2}{SNR_{proc,i}}, \qquad (39)$$

where c_1 [m^2] accounts for transmitter related noise, which is assumed to be 6 m, one sigma [12] and $SNR_{proc,i}$ [-] is the SNR of pre-processed signals. This includes the credit for non-linear processing, gain due to averaging, and also the debit due to blanking. The achievable 2DRMS positioning accuracy can now be calculated in the same way as was shown in Section 2.4.

4 Loran Signal Processing Toolbox

In an attempt to verify the presented models, numerical simulations of Loran signal processing were conducted. A basic Loran signal processing toolbox has been implemented in MATLAB™, which has the following features:

- Generation of Loran signals with the timing relations and amplitudes corresponding to a specified location (see Figure 1). Signal amplitudes are calculated using a ground wave propagation model based on Millington's method.
- Dual-rate transmitter blanking.
- Basic processing of simulated Loran signals according to Figure 7.

The toolbox implements all the basic Loran signal processing stages, which have been briefly described in Section 1.2.

5 Case Study

We will now demonstrate the use of the tools presented in this paper through a case study showing the impact of CRI on the Loran positioning performance from three different perspectives. First, the errors induced by unmitigated CRI are modelled at a particular location within the coverage area of

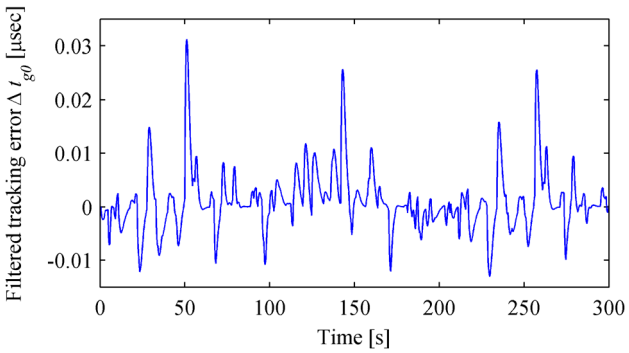

Figure 8: Filtered tracking error calculated according to the analytical method described in Section 3.

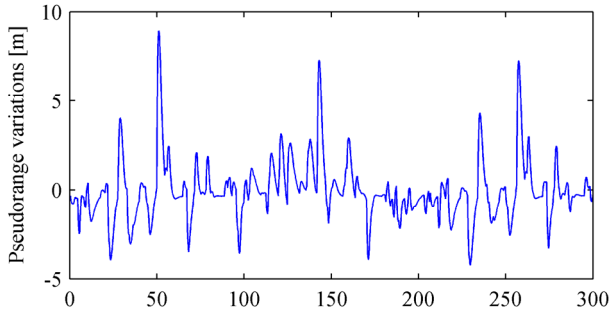

Figure 9: Pseudorange measurements (mean value subtracted) obtained by a numerical simulation using the Loran signal processing toolbox described briefly in Section 5.

the northwest European Loran system and the results are compared with the outputs of the Loran signal processing toolbox described above. The same model is then used to visualise the distribution of the CRI induced errors over the estimated coverage area[11] of the European system. The third example shows what price we have to pay when we decide to mitigate CRI through blanking.

5.1 Position Error Due to Unmitigated CRI at Harwich, UK

There are currently 9 operational Loran transmitters in northwest Europe. Coverage in eastern Europe is provided by a chain of 5 stations belonging to the Russian Chayka system, which broadcasts a signal that is compatible with Loran [1]. For simplicity, we will assume that the position solution is derived from the signals of the 6731 Lessay chain only, and also that the only sources of interference are the signals of the neighbouring 7499 Sylt chain. Signal timing and dual-rate blanking configurations of the stations used in this example can be found in Appendix D.

The exact location for the experiment is: 51.946856°N, 1.284991°E, Trinity House office building, Harwich, UK (see Figure 2). A snapshot of the Loran signals of the 6731 and 7499 chains as they would be received at this location can be seen in Figure 1.

Figure 4 in Section 2 shows a time plot of the filtered tracking error due to CRI for the 6731 Lessay station that spans over the whole overlap interval of the two GRIs (approx. 1009 s). This plot has been obtained by the analytical method

[11] region of sub-20 m accuracy (2DRMS) according to the traditional model, which doesn't respect CRI

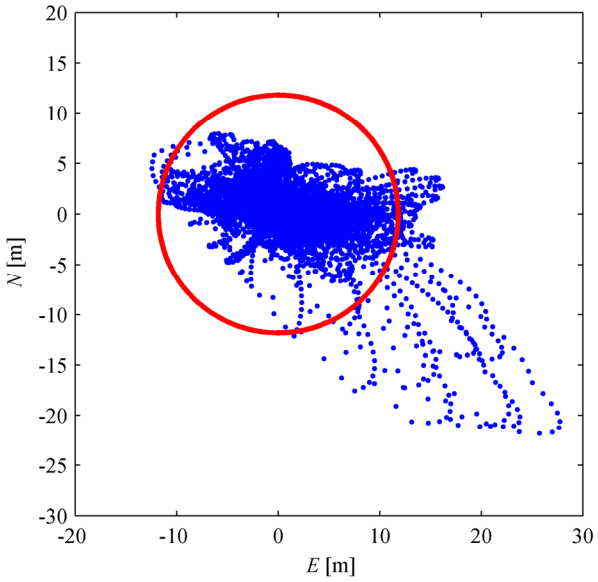

Figure 10: Simulated scatter plot; the origin corresponds to the location of the Trinity House office building, Harwich, UK; position solution based on the signals of the Lessay chain only.

described in this paper. The output filter used was a digital equivalent of a 2nd order Bessel filter with a bandwidth of 0.9 rad/s. This kind of filter was used as it provided the best fit to the data presented in [25]. In Figure 8, a detail of this plot is shown. For comparison, pseudorange data obtained by processing of simulated Loran signals are included in Figure 9. These signals were processed using the MATLAB toolbox described in section 5 - i.e. in a similar way as a real receiver would do. There is perfect agreement between the two plots and it can be seen that there are peak errors of approx. 9 m in the pseudorange measurements shown here.

GRI ID and Station Name	Mean Pseudorange Error [m]	Std. Deviation of Pseudorange Error [m]
6731 Lessay	0.36	1.67
6731 Soustons	7.67	18.94
6731 Anthorn	0.75	4.83
6731 Sylt	-1.20	5.48

Table 2: Pseudorange error statistics obtained by the semi-analytical method.

Further, pseudorange error statistics for all the stations used in the position solution were estimated in the way described earlier (see Table 2), and the 2DRMS error due to CRI was calculated using Equations 18, 19 and 15. This was shown to be:

$$\delta_{2DRMS} \doteq 11.7 \text{ m}.$$

Signal processing simulations were used to verify the calculated value of 2DRMS position error. Figure 10 shows a scatter plot obtained by processing of 1010 s of simulated Loran signals (approx. the overlap time). The plot was constructed by projecting the position measurements (in geodetic coordinates) into a local tangent plane with the origin corresponding to the true receiver position. The 2DRMS error calculated from these data is:

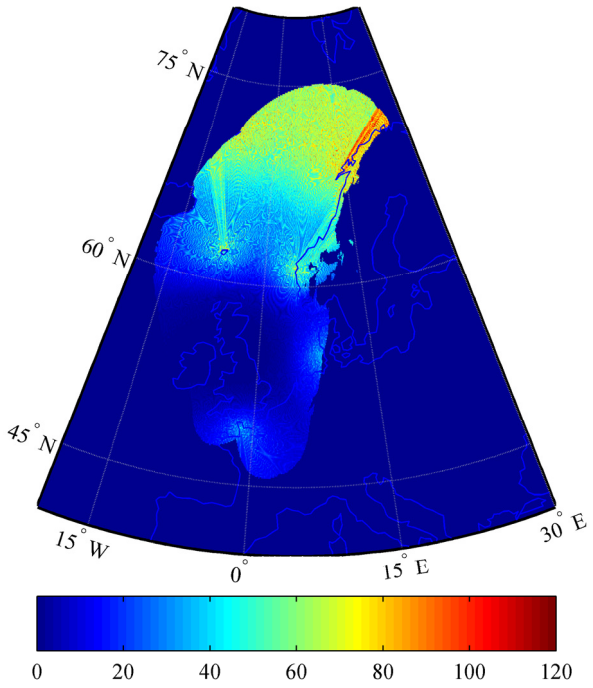

Figure 11: Standard deviation [m] of pseudorange measurement error due to unmitigated CRI for the 6731 Anthorn station.

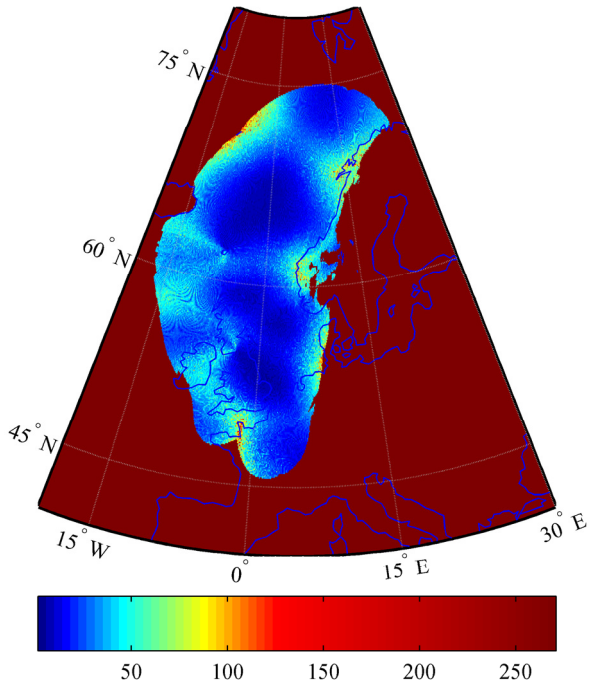

Figure 12: Position error [m] (2DRMS) due to unmitigated CRI.

$$\delta'_{2DRMS} \doteq 11.8 \text{ m}.$$

Again, the agreement between the semi-analytical and numeric approach is almost perfect. However, the scatter plot reveals *peak position errors of nearly 35 m*!

5.2 Position Error Due to Unmitigated CRI in Europe

We now use the model from Section 2 to evaluate the distribution and severity of CRI induced errors within the current European Loran network. Our transmission network will be formed by the 9 European transmitters (14 stations) configured into 4 chains as shown in Appendix D. The calculations will be performed only within the estimated coverage area of the European system (sub-20 m accuracy), obtained as explained in Section 5.3.

Figure 11 shows the standard deviation of pseudorange measurements error caused by unmitigated CRI for the 6731 Anthorn station. The adverse effect of other Loran stations operating on different GRIs is clearly seen in this figure. It is also interesting to note the fine structure of the image, which is a result of the phase dependence of the errors. As with Anthorn, we have estimated the standard deviations and mean values of the errors for all the other stations in our network. Based on these results, the component of positioning error due to CRI can be calculated in the same way as was shown in Section 2.4. For the current configuration of the transmission network, the CRI induced component of the positioning error is plotted in Figure 12. In the proximity of some stations this estimated error exceeds 250 m (2DRMS). Figure 13 shows the same plot, but the maximum displayed value in this figure is limited to 20 m, which corresponds[12] to the minimum accuracy requirement for maritime *Harbour Entrance and Approach* (HEA) [15]. We can clearly see that meeting the stringent eLoran accuracy performance standards cannot be achieved without implementing some CRI mitigation algorithms in eLoran receivers.

5.3 Impact of CRI Blanking on Achievable eLoran Accuracy in Europe

In this example study we demonstrate how the errors caused by unmitigated CRI can be eliminated through blanking and we evaluate the attendant blanking loss on individual Loran signals. Our transmission network will again be formed by the 14 European stations configured according to Appendix D. CRI originating from other Loran transmitters than those in Appendix D is not considered in this example.

Figure 14 shows predicted accuracy plot for our network calculated according to the traditional approach to coverage prediction, which does not take CRI into account. The maximum displayed value in this plot is limited to 20 m (minimum accuracy requirement for maritime HEA [15]). The calculations were performed as described in Section 3.3, except that the values of blanking loss were set to 0 for all the stations. The integration time required for tracking was set to 5 s and a 12 dB credit for non-linear processing was assumed. We used atmospheric noise at 99.7 percentile, which corresponds to the 99.7% minimum availability requirement for HEA [15].

[12] Note, however, that the plot does not include the effect of atmospheric noise.

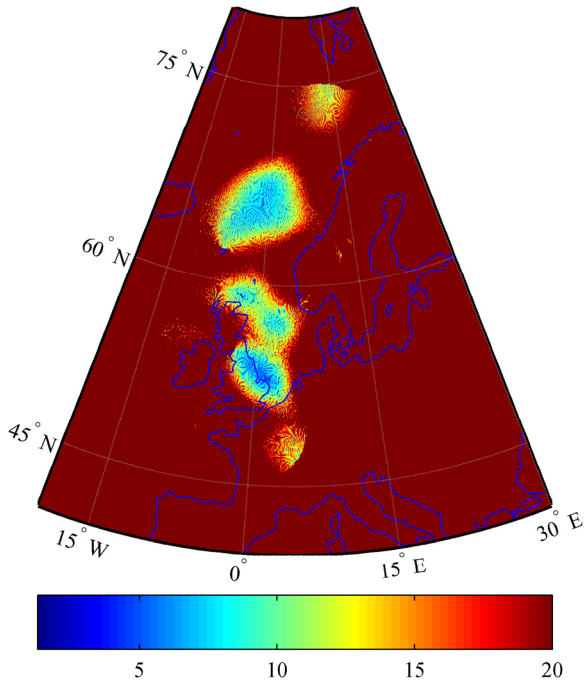

Figure 13: Position error (2DRMS) due to unmitigated CRI (within 20 m).

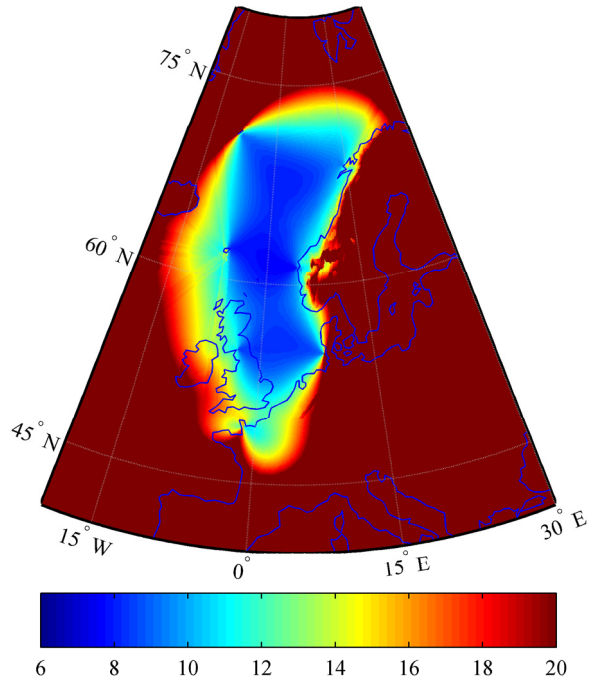

Figure 14: Accuracy [m] (2DRMS) within 20 m according to a traditional model; averaging 5 s, atmospheric noise at 99.7 percentile, SNR credit for non-linear processing 12 dB.

GRI ID and Station Name	$L_{b,DR,num}$ [%]	$L_{b,num}$ [%]	$L_{b,stat}$ [%]	$D_{b,approx}$ [dB]
6731 Lessay	0.00	32.81	32.81	1.7
6731 Soustons	0.00	36.65	36.65	2.0
6731 Anthorn	0.00	36.65	36.65	2.0
6731 Sylt	13.06	45.87	45.88	2.7
7001 Bø	10.87	49.10	49.11	2.9
7001 Jan Mayen	10.87	49.10	49.11	2.9
7001 Berlevag	0.00	41.43	41.43	2.3
7499 Sylt	0.00	37.97	37.98	2.1
7499 Lessay	14.54	52.51	52.53	3.2
7499 Værlandet	0.00	39.05	39.05	2.2
9007 Ejde	0.00	40.98	40.98	2.3
9007 Jan Mayen	0.00	36.86	36.86	2.0
9007 Bø	0.00	36.86	36.86	2.0
9007 Værlandet	13.06	50.19	50.21	3.0

Table 3: Blanking loss for the European stations; columns 2 – 3 show the blanking loss due to dual-rate blanking, and the total blanking loss respectively, obtained by the number-theoretic method; column 4 shows the total blanking loss obtained by the probabilistic method and column 5 is the approximate SNR debit due to blanking.

We now evaluate the blanking loss for each individual station resulting from discarding overlapping pulses from other chains of our network. Table 3 shows blanking loss values obtained by the number-theoretic method for one particular location and the average values obtained by the probabilistic method (both described in Section 3). We can see that there is almost perfect agreement between the two methods. This is due to the fact that all the GRIs in this example are mutually prime and for such signals the number of blanked pulses per overlap time shows very small or no variation with changing time alignment between the signals (recall Figure 5). No matter where we are, the number of overlapped pulses per overlap time will be practically the same and approximately equal to the average value, obtained by the probabilistic method (essentially Equation 26). For European chains, this simple method thus seems to be a convenient tool for analysing CRI issues.

Table 3 also shows the equivalent SNR debit due to blanking, which in this example ranges from 1.7 dB to 3.2 dB. If we incorporate the blanking loss values into our predictions, we can observe approximately 6% reduction in the region of sub-20 m accuracy, as can be seen in Figure 15 and Figure 16.

In this specific example, the rather large errors caused by uncompensated CRI are thus mitigated at the cost of a slight reduction in the estimated coverage area, calculated using the traditional model. However, we haven't taken into account CRI from other existing chains and we also haven't included sky wave borne CRI into our considerations yet. It is known [18] that CRI induced errors include significant components injected from distances exceeding 2500 kilometres. Under such conditions, blanking all the interfering pulses may prove ineffective due to excessive blanking loss and other approaches to CRI mitigation may need to be sought.

6 Future Work

Although this paper attempts to provide an in-depth view of the impact of CRI on Loran positioning performance, a number of assumptions and simplifications have been introduced and further investigations are needed.

As for the models presented in this paper, their biggest drawback at the moment seems to be that they do not take sky waves into account. These are particularly significant

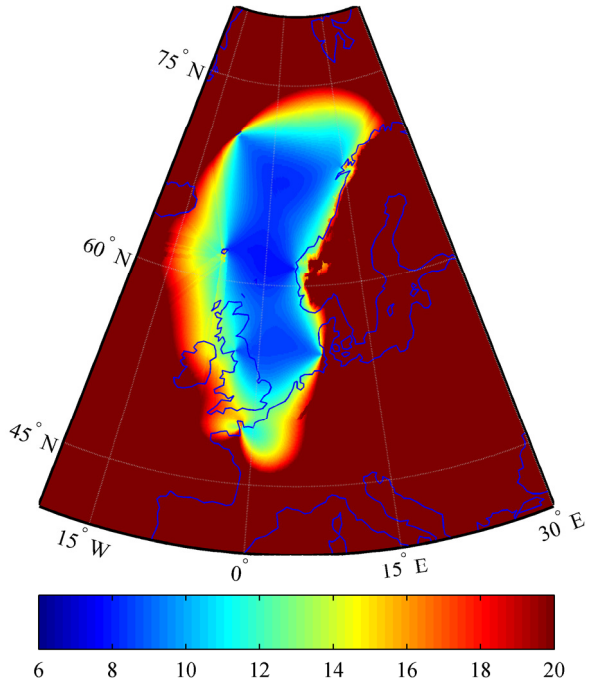

Figure 15: Accuracy [m] (2DRMS) within 20 m including the effects of blanking; averaging 5 s, atmospheric noise at 99.7 percentile, SNR credit for non-linear processing 12 dB.

during night-time hours [18] when they can travel long distance with only moderate attenuation. Therefore, *sky wave borne CRI* should definitely be included into the analysis in future.

In terms of the benefits delivered by current eLoran technology, the effectiveness of other advanced *signal processing methods for CRI mitigation* [16], such as cancelling, should be assessed.

Further potential for mitigation of the negative effects of CRI lies in possible alterations to the signal specification. *Changes to phase-codes*, for example, have been suggested many times before [21] and the methods presented in this paper could be used to confirm the benefits to be gained by introducing these changes. Similarly, with a *GRI reassignment* in Europe which should probably be done with a higher emphasis on CRI mitigation.

7 Conclusions

This analysis has proven that unmitigated CRI is a serious source of interference to Loran. The analytical results obtained seem to be in accordance with the experimental data presented in [18], where the author states, that uncompensated CRI adds substantial offsets to Loran timing measurements that are of *"more than academic importance"* and can be as high as 100 ns.

CRI might also be a threat to eLoran – the errors introduced by this kind of interference change rapidly in time and they are also highly uncorrelated in the position domain, therefore they can be compensated neither by differential corrections nor any surveys. Introducing measures to mitigate CRI should be the top priority in the design of the new eLoran system.

In this paper, we have analysed the possibility of mitigating CRI within the European Loran network through blanking the

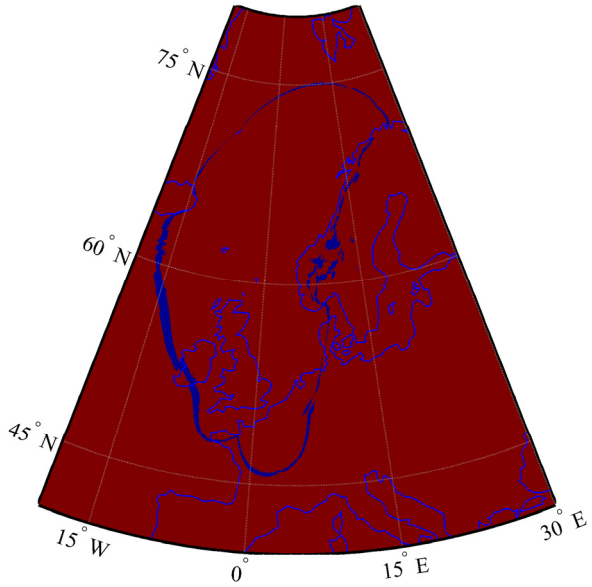

Figure 16: Difference in the regions of sub-20 m accuracy - traditional model (no CRI considerations) vs. blanking.

interfering pulses at the receiver end. We have shown that for some stations over 50% of pulses have to be discarded. In reality, this number is likely to be even higher, as we have not accounted for the effects of sky wave borne CRI and CRI from more distant transmitters.

It is apparent that the measures for CRI mitigation need to be taken on both the receiver and system design sides. Both of these aspects will be explored in further work.

Acknowledgements

This work is sponsored by a grant from the Corporation of Trinity House.

References

[1] European transmitters. GLAs R&RNAV website, 2009.

[2] J. Šafář. eLoran - Společník družicové navigace? *Slaboproudý obzor*, 2:9–15, 2009. (Czech).

[3] J. Šafář, P. Williams, and S. Gug. Group Repetition Interval Selection for eLoran. In *Proceedings of the Royal Institute of Navigation (RIN) NAV08/ International Loran Association 37th Annual Meeting*, 2008.

[4] C.O.L. Boyce. *Atmospheric Noise Mitigation for LORAN*. PhD thesis, Stanford University, 2007.

[5] J. Clynch. The Hunt for RFI - Unjamming a Coast Harbor, January 2003.

[6] Henry D. Friedman. Coincidence of pulse trains. *Journal of Applied Physics*, 25(8):1001–1005, Aug 1954.

[7] A. Grant, P. Williams, N. Ward, and S. Basker. GPS Jamming and the Impact on Maritime Navigation. *The Journal of Navigation*, 62:173–187, 2009.

[8] International Loran Association. *Enhanced Loran (eLoran) Definition Document*, 2007. v. 1.0.

[9] International Telecommunication Union. *ITU-R P.372-8, Radio Noise*, 2003.

[10] John A. Volpe National Transportation System Center. *Vulnerability Assessment of the Transportation Infrastructure Relying on the Global Positioning System*, 2001.

[11] G. Johnson, M. Wiggins, P. F. Swaszek, L. Hartshorn, and R. Hartnett. Possible Optimizations for the US Loran System. In *Proc. IEEE/ION Position, Location, And Navigation Symposium*, pages 695–704, April 25–27, 2006.

[12] S. Lo, B. Peterson, C.O.L. Boyce, and P. Enge. Loran Coverage Availability Simulation Tool. In *Proceedings of the Royal Institute of Navigation (RIN) NAV08/ International Loran Association 37th Annual Meeting*, 2008.

[13] Sherman Lo, Ben Peterson, Per Enge, Robert Wenzel, Booz Allen Hamilton, G. T. Gunther, Peter Morris, and Kevin Carroll. Loran integrity analysis for required navigation performance 0.3. Presented at the 5th International Symposium on Integration of LORAN-C/Eurofix and EGNOS/Galileo, Munich, Germany, 2004.

[14] K. S. Miller and R. J. Schwarz. On the interference of pulse trains. *Journal of Applied Physics*, 24(8):1032–1036, Aug 1953.

[15] Mitchell J. Narins. Loran's Capability to Mitigate the Impact of a GPS Outage on GPS Position, Navigation, and Time Applications. Technical report, Federal Aviation Administration, 2004.

[16] W. Pelgrum. *New Potential of Low-Frequency Radionavigation in the 21st Century*. PhD thesis, TU Delft, Delft, 2006.

[17] Wouter Pelgrum. Noise - From a Receiver Perspective. In *Proceedings of the 34th Annual Convention and Technical Symposium of the International Loran Association*, 2005.

[18] P. W. Schick. Cross-Rate Interference Effects and Differential Loran Operation. In *Proceedings of the 25th Annual Technical Symposium, Wild Goose Association*, 1996.

[19] A. G. Self and B. G. Smith. Intercept time and its prediction. *IEE Proceedings F Communications, Radar and Signal Processing*, 132(4):215–220, July 1985.

[20] S. Stein and D. Johansen. A statistical description of coincidences among random pulse trains. *Proceedings of the IRE*, 46(5):827–830, May 1958.

[21] P.F. Swaszek, G. Johnson, R. Shalaev, and R. Hartnett. Loran phase codes, revisited. In *Proc. IEEE/ION Position, Location and Navigation Symposium*, pages 800–809, 2008.

[22] United States Coast Guard. *Specification of the Transmitted LORAN-C Signal*, 1994. COMDTINST M16562.4A.

[23] Frank van Diggelen. GPS Accuracy: Lies, Damn Lies, and Statistics. GPS World web-site, November 1998.

[24] A. I. Williams. *Prediction of the Coverage and Performance of the Datatrak Low-Frequency Tracking System*. PhD thesis, University of Wales Bangor, 2004.

[25] M.J. Zeltser and M.B. El-Arini. The Impact of Cross-Rate Interference on LORAN-C Receivers. AES-21(1):36–46, 1985.

Appendix A

Matrix $\mathbf{A}$, the *direction cosine matrix,* also called the *geometry matrix,* contains the cosines and sines of the bearings β_i of the individual stations from the receiver:

$$\mathbf{A} = \begin{pmatrix} \sin\beta_1 & \cos\beta_1 & 1 \\ \vdots & \vdots & \vdots \\ \sin\beta_K & \cos\beta_K & 1 \end{pmatrix}. \qquad \text{(A.1)}$$

Appendix B

After the position solution algorithm described in Section 4 has converged, $\Delta\boldsymbol{\rho}$ can be considered as a vector of measurement errors and $\Delta\mathbf{u}$ as the position error due to these measurement errors. The mean and variance of the errors in user's position can be expressed as functions of the direction cosine matrix, weight matrix, and the variance of the pseudorange measurements.

The mean position error can be obtained directly from Equation 10, where the only random variable on the right hand side is $\Delta\boldsymbol{\rho}$:

$$\mathrm{E}[\Delta\mathbf{u}] = \mathrm{E}\left[\left(\mathbf{A}^{\mathrm{T}}\mathbf{W}\mathbf{A}\right)^{-1}\mathbf{A}^{\mathrm{T}}\mathbf{W}\Delta\boldsymbol{\rho}\right],$$

$$\mathrm{E}[\Delta\mathbf{u}] = \left(\mathbf{A}^{\mathrm{T}}\mathbf{W}\mathbf{A}\right)^{-1}\mathbf{A}^{\mathrm{T}}\mathbf{W}\,\mathrm{E}[\Delta\boldsymbol{\rho}]. \qquad \text{(B.1)}$$

The variance of the position error can be calculated using the well-known identity:

$$\mathrm{var}(\mathbf{B}\mathbf{x}) = \mathbf{B}\,\mathrm{var}(\mathbf{x})\mathbf{B}^{\mathrm{T}}, \qquad \text{(B.2)}$$

where $\mathbf{x}$ is a random $n \times 1$ vector and $\mathbf{B}$ is an $m \times n$ matrix. Applying this to Equation 10 gives:

$$\mathrm{var}(\Delta\mathbf{u}) = \left(\mathbf{A}^{\mathrm{T}}\mathbf{W}\mathbf{A}\right)^{-1}\mathbf{A}^{\mathrm{T}}\mathbf{W}\underbrace{\mathrm{var}(\Delta\boldsymbol{\rho})}_{\mathbf{R}}\mathbf{W}^{\mathrm{T}}\mathbf{A}\left(\mathbf{A}^{\mathrm{T}}\mathbf{W}^{\mathrm{T}}\mathbf{A}\right)^{-1}. \qquad \text{(B.3)}$$

The position error variance is minimised when the weight matrix is equal to the inverse of the measurement covariance matrix:

$$\mathbf{W} \equiv \mathbf{R}^{-1}. \qquad \text{(B.4)}$$

Under this assumption, the expression for the variance reduces to the following form:

$$\mathrm{var}(\Delta\mathbf{u}) = \left(\mathbf{A}^{\mathrm{T}}\mathbf{R}^{-1}\mathbf{A}\right)^{-1}. \qquad \text{(B.5)}$$

Appendix C

In the Loran Signal Specification [22], the Signal-to-Noise Ratio (SNR) is defined as the ratio of the RMS amplitude of the Loran pulse at the standard sampling point (SSP) [13], V_{SSP}, to the RMS value of the noise, V_N, present at that time. In engineering applications, however, SNR is normally expressed as a power ratio. We therefore write:

$$SNR_{dB} = 10\log_{10}\frac{P_{SSP}}{P_N} = 20\log_{10}\frac{V_{SSP}}{V_N}. \qquad \text{(C.1)}$$

[13] The SSP is the envelope value 25 μsec into the Loran pulse.

If we use n pulses from a specific station in our measurement, the power of the desired signal is increased n^2 times, whereas the power of noise increases only n times, as the noise in successive signal samples is assumed to be uncorrelated:

$$SNR_{dB,n} = 10\log_{10}\frac{n^2 P_{SSP}}{nP_N} = \underbrace{10\log_{10} n}_{G_a} + SNR_{dB}. \qquad \text{(C.2)}$$

The term denoted by G_a is the *processing gain due to averaging*; n depends on the averaging time used and the GRI of the tracked signal. If some fraction of pulses, L_b, is blanked then this gain has to be reduced accordingly:

$$G_a' = 10\log_{10}\lfloor(1-L_b)n\rfloor \approx G_a \underbrace{-10\log_{10}\frac{1}{1-L_b}}_{\substack{\text{approx. SNR debit} \\ \text{due to blanking}}}. \qquad \text{(C.3)}$$

$\lfloor x \rfloor$ denotes rounding to the nearest integer smaller than x.

Appendix D

GRI ID and Station Name	Emission Delay [μs]	Dual-Rate Blanking
6731 Lessay	0	Priority 6731
6731 Soustons	13 000	Not dual-rated
6731 Anthorn	27 300	Not dual-rated
6731 Sylt	42 100	Priority 7499
7001 Bø	0	Priority 9007
7001 Jan Mayen	14 100	Priority 9007
7001 Berlevag	29 100	Not dual-rated
7499 Sylt	0	Priority 7499
7499 Lessay	14 100	Priority 6731
7499 Værlandet	29 500	Priority 7499
9007 Ejde	0	Not dual-rated
9007 Jan Mayen	14 200	Priority 9007
9007 Bø	28 000	Priority 9007
9007 Værlandet	41 100	Priority 7499

Table D.1: European Loran stations.